International Journal of Thermal Sciences 48 (2009) 1843–1852

Contents lists available at ScienceDirect

International Journal of Thermal Sciences

journal homepage: www.elsevier.com/locate/ijts

Scaling of unsteady natural convection boundary layers with a non-instantaneous initiation

John C. Patterson [a,*], Chengwang Lei [a], Steve W. Armfield [b], Wenxian Lin [a]

[a] School of Engineering, James Cook University, Townsville QLD 4811, Australia
[b] School of Aerospace, Mechanical and Mechatronic Engineering, The University of Sydney, Sydney NSW 2006, Australia

ARTICLE INFO

Article history:
Received 2 September 2008
Received in revised form
12 February 2009
Accepted 24 February 2009
Available online 17 April 2009

Keywords:
Natural convection
Scaling
Boundary layer

ABSTRACT

A scaling analysis is presented for the transient boundary layer established on a vertical wall following non-instantaneous heating in the form of an imposed wall temperature which increases linearly up to a prescribed steady value over a prescribed time. The scaling analysis is verified by comparison with numerical solutions of the full equations of motion and energy. The analysis reveals that, if the period of temperature growth on the wall is sufficiently long, the boundary layer reaches a quasi-steady state before the temperature growth is completed. In this mode the thermal boundary layer at first grows in thickness and then contracts with increasing time, and the fluid acceleration also changes character. If the wall temperature growth period is sufficiently short, the boundary layer commences differently, but after the wall temperature growth is completed, the boundary layer develops as though the start up had been instantaneous. In both cases, the ultimate steady state is the same as if the start up had been instantaneous; however the different transient nature may have implications for the stability of the boundary layer or of the subsequent development of the flow in a cavity of which the wall is one boundary.

1. Introduction

The flow induced adjacent to a heated vertical wall is one of the classical problems of heat and mass transport, with relevance to both engineering applications and fundamental fluid mechanics. Of particular interest is the configuration of a suddenly heated wall in an initially stationary and isothermal ambient fluid; an understanding of the development of the subsequent flow is the basis for the design of heat exchangers and many other industrial applications, as well as providing insight into the properties of the developing boundary layer. Consequently, considerable attention has been paid to this problem in the literature. Much of the focus of this has been in the context of the way in which the boundary layer changes its state from a one dimensional unsteady [25] to a two dimensional steady flow [21] by means of the passage of the Leading Edge Effect (LEE), and a number of papers, including those of [9–14], dealt with various aspects of this question for both suddenly applied isothermal and isoflux wall boundary conditions. The issue was also discussed in the context of a vertical wall in a rectangular cavity by [7,22,26,27].

One of the important issues in this discussion was a determination of the time at which the boundary layer reached steady state. The accurate calculation of this, according to the hypothesis of [7] and supported by the experiments described in [22] for sudden isothermal heating, involved the calculation of the wave speeds of the fastest travelling waves on the boundary layer resulting from the perturbation of the layer at start up.

A simpler approach to the development of the flow from sudden isothermal heating is available by means of scaling arguments similar to those described by [23], in which simple scaling balances for the various stages of the flow development in a differentially heated cavity were developed, including the start up of the boundary layer on the heated wall, the properties of the resulting intrusions, and the approach to a steady state. The scales for the boundary layer were verified in a detailed way by [16,17,20]. Similarly, scales for the development of the boundary layer for sudden isoflux heating were described by [5], and these scales were verified by detailed comparisons with numerical simulation over a range of forcing parameters.

These flows may easily be shown to depend on the Rayleigh number *Ra*, which measures the strength of the heating, and the Prandtl number *Pr*, which defines the relative diffusion of momentum and heat in the fluid. These parameters are defined later. For the case of a rectangular cavity, the flows also depend on the aspect ratio [20].

All of this scaling work was done in the context of an instantaneous, that is, a step function, application of either the isothermal

* Corresponding author. Tel.: +61 7 4781 5083; fax: +61 7 4781 6788.
E-mail address: john.patterson@jcu.edu.au (J.C. Patterson).

1290-0729/$ – see front matter © 2009 Elsevier Masson SAS. All rights reserved.
doi:10.1016/j.ijthermalsci.2009.02.023

Nomenclature

g	Acceleration due to gravity
H	Vertical length scale
Ra	Rayleigh number
Pr	Prandtl number
T_0	*Initial* temperature
T_{Wall}	Wall *temperature*
T	Fluid temperature
t	Time
t_W	Ramp time
t_C	Boundary layer steady state time for an instantaneous start up
t_0	Quasi-steady state time
u,υ	Horizontal and vertical velocities
υ_{max}	Maximum vertical velocity
x,y	Horizontal and vertical coordinates
X,Y	Horizontal and vertical extent of the computation domain
ν	Kinematic viscosity
κ	Thermal diffusivity
β	Coefficient of thermal expansion
ΔT	Final imposed wall temperature difference
δ_T	Thermal boundary layer thickness scale
δ_{T0}	Thermal boundary layer thickness scale at time t_0
δ_{TW}	Thermal boundary layer thickness scale at time t_W
δ_ν	Viscous boundary layer thickness scale
$\delta_{\nu 0}$	Viscous boundary layer thickness scale at time t_0
$\delta_{\nu W}$	Viscous boundary layer thickness at time t_W
δ	Scale of the position of the velocity maximum relative to the thermal boundary layer thickness
δ_0	*Scale* of the position of the velocity maximum relative to the thermal boundary layer thickness at time t_0
δ_W	*Scale* of the position of the velocity maximum relative to the thermal boundary layer thickness at time t_W
υ_m	Vertical velocity scale
υ_{m0}	Vertical velocity scale at time t_0
υ_{mW}	Vertical velocity at time t_W
Δt	Computational time step
$\Delta x,\Delta y$	Computational horizontal and vertical mesh size

or isoflux boundary condition on the vertical wall. The reality is that this is not possible to achieve physically, and thus consideration needs to be given to the case where the heating is applied over some non-zero time period. Further, the verification of scaling analysis has normally been carried out for fixed Pr, and the dependence on varying Pr has to date not been properly tested.

It is worth noting that for the infinite plate version of all of these transient flows closed form solutions may be available. These are often complex and the dependence of the flow on the various parameters is not obvious; one of the benefits of a scaling analysis of the flow is that the various mechanisms governing the flow are revealed and the parameter dependence is clarified.

In this paper, new scaling for the development of the boundary layers on a vertical wall with isothermal heating applied over a time scale t_W is described. The analysis is restricted to the case with $Pr \gg 1$. The scaling properly incorporates the effects of varying Pr by examining the balances in more detail than previously considered. The resultant time, velocity and length scales for the boundary layer both during and following the ramp time for isothermal heating are verified by numerical simulations. These verifications are confirmed over a range of parameter values.

A companion paper will deal with the case of the Pr dependence of the developing flow for the case of instantaneous isothermal heating [19]. A similar scaling approach for the steady state flow near a vertical wall with a constant applied heat flux was reported by [1].

2. Formulation

Under consideration are the flow and temperature fields adjacent to a heated wall, as sketched in Fig. 1(a). The scaling is focused on the flow in the boundary layer, sufficiently far from horizontal boundaries or the leading edge. The full equations of momentum, continuity and energy, under the usual Boussinesq assumption, are:

$$\frac{\partial u}{\partial t} + u\frac{\partial u}{\partial x} + \upsilon\frac{\partial u}{\partial y} = -\frac{1}{\rho}\frac{\partial p}{\partial x} + \nu\left(\frac{\partial^2 u}{\partial x^2} + \frac{\partial^2 u}{\partial y^2}\right) \tag{1}$$

$$\frac{\partial \upsilon}{\partial t} + u\frac{\partial \upsilon}{\partial x} + \upsilon\frac{\partial \upsilon}{\partial y} = -\frac{1}{\rho}\frac{\partial p}{\partial y} + \nu\left(\frac{\partial^2 \upsilon}{\partial x^2} + \frac{\partial^2 \upsilon}{\partial y^2}\right) + g\beta(T - T_0) \tag{2}$$

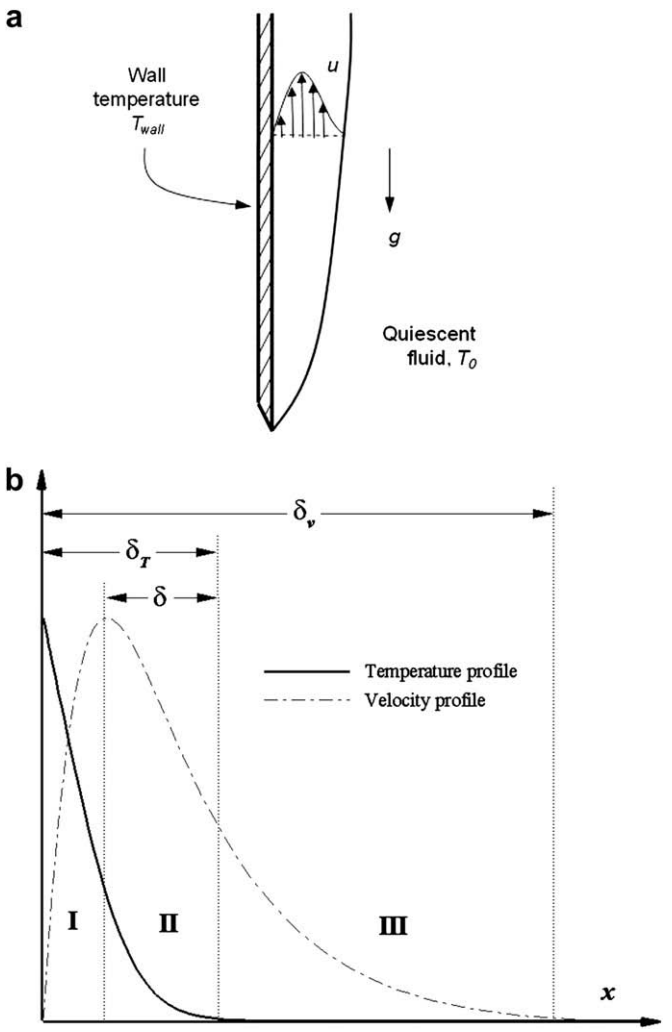

Fig. 1. (a) A sketch of the flow adjacent to a semi infinite heated wall. (b) A schematic of the temperature and velocity profiles normal to the vertical wall. The thermal boundary layer is $O(\delta_T)$, the viscous boundary layer is $O(\delta_\nu)$ and δ is the scale for the distance between the maximum velocity and δ_T. The regions I, II and III are as shown on the figure.

$$\frac{\partial u}{\partial x}+\frac{\partial v}{\partial y}=0 \tag{3}$$

$$\frac{\partial T}{\partial t}+u\frac{\partial T}{\partial x}+v\frac{\partial T}{\partial y}=\kappa\left(\frac{\partial^2 T}{\partial x^2}+\frac{\partial^2 T}{\partial y^2}\right) \tag{4}$$

Initially, the fluid is quiescent and isothermal at temperature T_0. The initial conditions for velocity and temperature are then

$$\left.\begin{array}{l} u=v=0 \\ T=T_0 \end{array}\right\}\ \forall\, x,\, y\ t<0 \tag{5}$$

On a semi infinite vertical wall, the velocity boundary conditions are

$$u=v=0 \quad \left.\begin{array}{l} x=0,\ \ y\geq 0 \\ x\to\infty \end{array}\right\} t\geq 0 \tag{6}$$

The temperature boundary condition on the wall is specified by the final wall temperature $T_0+\Delta T$ and the time t_W over which the wall temperature increases linearly from the initial value T_0 to the final value, as a ramp function. The temperature far from the wall is maintained at T_0 Thus

$$\left.\begin{array}{l} T=T_0 \quad x=0,\ \ t<0 \\ T=T_0+\frac{t}{t_W}\Delta T \quad x=0,\ \ 0\leq t\leq t_W \\ T=T_0+\Delta T \quad x=0,\ \ t_W<t \\ T=T_0 \quad x\to\infty,\ \ \forall\, t \end{array}\right\} \tag{7}$$

Under the usual boundary layer assumptions, the equations become:

$$\frac{\partial v}{\partial t}+v\frac{\partial v}{\partial y}=\nu\frac{\partial^2 v}{\partial x^2}+g\beta(T-T_0) \tag{8}$$

$$\frac{\partial T}{\partial t}+v\frac{\partial T}{\partial y}=\kappa\frac{\partial^2 T}{\partial x^2} \tag{9}$$

with appropriate boundary conditions extracted from (5)–(7).

It is easily shown from dimensional analysis that the flow is governed by two non dimensional parameters, the Rayleigh number *Ra* and the Prandtl number *Pr*, where

$$Ra=\frac{g\beta\Delta T H^3}{\nu\kappa} \tag{10}$$

and

$$Pr=\frac{\nu}{\kappa} \tag{11}$$

where H is an arbitrary length scale, which would normally be associated with the length of the wall in the cavity case.

3. Scaling analysis

The basic procedures described in [23] are followed here, modified appropriately for the case of non-instantaneous heating and to include the dependence on *Pr* correctly by examining in more detail the balances between the various terms of the boundary layer equations (8) and (9).

It is easily shown that for sufficiently small time, the convection term of (9) is very much less than the unsteady term. Consequently, initially heat is conducted into the fluid from the heated wall, forming a thermal boundary layer of thickness $O(\delta_T)$ where, from (9).

$$\delta_T\sim\kappa^{1/2}t^{1/2} \tag{12}$$

The resulting buoyancy term in the vertical momentum equation (8) is $O(g\beta\Delta T t/t_W)$, so long as $t<t_W$. This buoyancy accelerates the heated fluid over the thickness δ_T only. Over that scale, the ratio of the inertial and viscous terms in the vertical momentum equation is $O(\ (v_m\ /\ t)\ /(\nu v_m\ /\ \delta_T^2))$ where v_m is the vertical velocity scale in the boundary layer. Using (12), this ratio is less than 1 for $Pr\gg 1$, and the correct balance in this region is between buoyancy and viscosity.

The original scaling of [23] simply balanced these two terms to obtain (for the instantaneous start up) a velocity scale in the boundary layer. However, to properly incorporate the effects of variable *Pr* it is necessary to examine in more detail the structure of the boundary layer.

First, the temperature will decrease from its wall value to zero in the interior, over a distance $O(\delta_T)$. The accelerating fluid must have zero velocity at the wall, rise to a maximum and fall to zero in the interior. The peak velocity must occur within δ_T, and there will be non-zero velocity beyond δ_T where the fluid is driven by the diffusion of momentum by viscosity from the region accelerated by buoyancy. The full thickness of the region over which the velocity occurs is some length scale $O(\delta_\nu)$, denoted the viscous boundary layer. The form of the temperature and velocity profiles is shown in the schematic in Fig. 1(b); the length scale δ is the distance between the maximum velocity and the extent of the thermal boundary layer. With increasing *Pr*, the thickness of the viscous boundary layer δ_ν increases relative to the thickness of the thermal boundary layer δ_T.

It is now instructive to examine the balances in each of the three regions I, II and III shown in Fig. 1(b).

In both regions I and II, the initial balance in the vertical momentum equation is between the buoyancy and viscous terms, so long as the scale (12) holds. Thus, in region I, $0\sim\nu\partial^2 v/\partial x^2+g\beta T$. Integrating this across region I, that is between 0 and $(\delta_T-\delta)$, noting that $\partial v/\partial x\sim 0$ at $(\delta_T-\delta)$, and approximating $\int_0^{\delta_T-\delta}T\mathrm{d}x$ $\Delta T(t/t_W)(\delta_T-\delta)$ yields

$$v_m\sim\frac{g\beta\Delta T}{\nu}\frac{t}{t_W}(\delta_T-\delta)^2 \tag{13}$$

In region II, the first integral is taken between $(\delta_T-\delta)$ and δ_T, again noting that $\partial v/\partial x\sim 0$ at $(\delta_T-\delta)$, approximating $\partial v/\partial x|_{\delta_T}\sim v_m/(\delta_\nu-\delta_T+\delta)$ and $\int_{\delta_T-\delta}^{\delta_T}T\mathrm{d}x\sim\Delta T(t/t_W)\delta$ yields

$$v_m\sim\frac{g\beta\Delta T}{\nu}\frac{t}{t_W}\delta(\delta_\nu-\delta_T+\delta) \tag{14}$$

Here, the scale $(\delta_\nu-\delta_T+\delta)$ is used in the viscous term as this is the length over which the velocity reduces from its maximum value to zero.

These two velocity scales must be the same, so

$$v_m\sim\frac{g\beta\Delta T}{\nu}(\delta_T-\delta)^2\frac{t}{t_W}\sim\frac{g\beta\Delta T}{\nu}\delta(\delta_\nu-\delta_T+\delta)\frac{t}{t_W}\quad\text{or}\quad\delta\sim\frac{\delta_T^2}{\delta_\nu+\delta_T} \tag{15}$$

In region III, the flow is driven solely by the diffusion of momentum from region II. The appropriate balance here is between the unsteady term and the viscous term, so that $v_m/t\sim\nu v_m/\delta_\nu^2$, leading to

$$\delta_\nu\sim\nu^{1/2}t^{1/2}\sim Pr^{1/2}\delta_T \tag{16}$$

where in (16) the viscous term is taken over the full viscous boundary layer width. Then, from (10), $\delta\sim\delta_T/(1+Pr^{1/2})$ and consequently the velocity scale is, from (13) or (14)

$$v_m \sim \frac{Ra\kappa^2}{H^3}\frac{t^2}{t_W}\left(1-\frac{1}{1+Pr^{1/2}}\right)^2 \tag{17}$$

The flow in the period that the initial thermal balance is between conduction and unsteady temperature growth is then described by the length scales (12) and (16), and the velocity scale (17). The temperature is described by the scale $O(\Delta T t/t_W)$, so long as $t < t_W$.

The boundary layer flow is also convecting heat away, and the boundary layer growth will change character when the convection balances conduction, that is at time t_0 when $v_m \Delta T(t_0/t_W)/H \sim \kappa \Delta T(t_0/t_W)/{\delta_T}^2$ where v_m and δ_T are evaluated at t_0. This gives

$$t_0 \sim \frac{H^{4/3} t_W^{1/3}}{Ra^{1/3}\kappa^{2/3}\left(1-\frac{1}{1+Pr^{1/2}}\right)^{2/3}} \tag{18}$$

so long as $t_0 < t_W$. At this time the boundary layer will have reached a quasi-steady state; the original thermal balance between heat conduction and temperature growth no longer holds and the further heating which continues since $t_0 < t_W$ simply accelerates the fluid sufficiently to carry the additional heat away.

The requirement that $t_0 < t_W$ may be shown to be equivalent to the condition that

$$t_W > \frac{H^2}{Ra^{1/2}\kappa\left(1-\frac{1}{1+Pr^{1/2}}\right)} \tag{19}$$

This time scale is the same as the time scale t_C that an instantaneously started boundary layer will reach the same conduction – convection balance [19]. Thus, if $t_W < t_C$ the increasing heating has finished before the boundary layer has reached the quasi-steady state. Further, the velocity and boundary layer thickness scales at t_W are identical to those from the instantaneously started boundary layer at that time. In other words, if $t_W < t_C$, the boundary layer will subsequently follow the same development as the instantaneous case and become steady at t_C, and the scales will be identical to the instantaneous heating case; the boundary layer will not be affected at all by the presence of the ramp. That outcome is intuitively expected; if the ramp time is sufficiently short, the result will be the same as though the start up were instantaneous.

On the other hand, if $t_W > t_C$ then $t_0 < t_W$ and the boundary layer will reach a quasi-steady state at t_0, and for $t_0 < t < t_W$, the boundary layer will continue to develop, governed by a balance between convection and conduction. Thus, for $t_0 < t < t_W$, $v_m \Delta T(t/t_W)/H \sim \kappa \Delta T(t/t_W)/\delta_T^2$ where now δ_T is no longer governed by (12). This gives

$$v_m \sim \frac{\kappa H}{\delta_T^2} \tag{20}$$

The same balances between buoyancy and viscosity still apply in regions I and II, so that (15) applies. Further, since the boundary layer is in a quasi-steady state, the balance in region III is between advection and diffusion of momentum, so that

$$v_m \sim \frac{\nu H}{\delta_\nu^2} \tag{21}$$

and again $\delta \sim \delta_T/1+Pr^{1/2}$.

Using this result the velocity given by the balance in region I is $v_m \sim (g\beta\Delta T{\delta_T}^2/\nu)(1-1/(1+\mathrm{Pr}^{1/2}))^2(t/t_W)$. Together with (20), a scale for δ_T may be obtained

$$\delta_T \sim \frac{H}{Ra^{1/4}\left(1-\frac{1}{1+Pr^{1/2}}\right)^{1/2}}\left(\frac{t_W}{t}\right)^{1/4} \tag{22}$$

and a corresponding scale for v_m

$$v_m \sim \frac{Ra^{1/2}\kappa}{H}\left(1-\frac{1}{1+Pr^{1/2}}\right)\left(\frac{t}{t_W}\right)^{1/2} \tag{23}$$

Corresponding scales for the viscous boundary layer thickness δ_ν and the position of the velocity maximum $(\delta_T - \delta)$ are readily obtained. It is seen from (22) and (23) that, in this quasi-steady stage of the boundary layer development, the velocity increases, but the boundary layer thickness decreases with time. At $t \sim t_W$, the boundary layer becomes steady, with thickness δ_T and velocity v_m given by

$$\delta_{TW} \sim \frac{H}{Ra^{1/4}\left(1-\frac{1}{1+Pr^{1/2}}\right)^{1/2}} \tag{24}$$

$$v_{mW} \sim \frac{Ra^{1/2}\kappa}{H}\left(1-\frac{1}{1+Pr^{1/2}}\right) \tag{25}$$

In summary, if $t_0 < t_W$ the boundary layer grows and accelerates according to (12) and (17) until time t_0; it then contracts but accelerates further in a quasi steady mode until t_W, following (22) and (23). For $t > t_W$, the flow is steady and is described by (24) and (25). For $t_0 > t_W$ the boundary layer follows (12) and (17) until the end of the ramp at $t \sim t_W$. At t_W, the flow and temperature fields are the same as for an instantaneous start up at the corresponding time, and the further development beyond t_W is identical to that for an instantaneous start up [19].

4. Numerical procedures

To verify the various scales, numerical solution of the full equations of motion and energy are obtained for a range of Ra and Pr values, and the results, scaled by non dimensionalised forms of the various scale values above, are shown to approximately collapse onto a single line. In the following, time, velocity and length are scaled by H^2/κ, κ/H and H respectively, and the temperature difference from T_0 is scaled by ΔT.

The equations are solved on a domain $-0.2 \le y \le Y$, $0 \le x \le X$ where X and Y are the non dimensional width and non dimensional height respectively. For $Pr = 7$, the width is set to $X = 0.5$ and the height to $Y = 1.5$. For the remaining Pr values, $X = 2.0$ and $Y = 6.0$. The origin of the coordinate system is located at the leading edge of the heated plate, at $x = 0$, $y = 0$. The increased width for the larger Pr values is necessary to accommodate the increased width of the viscous boundary layer. Domain dependency tests were carried out to ensure that the far field boundary conditions were not significantly affecting the detailed results presented below. The following boundary conditions, in non dimensional form, are applied

$$\left.\begin{array}{l} u = v = 0, \ \text{for } x = 0, \ y \ge 0 \\ T = \frac{t}{t_W}, \ \text{for } x = 0, \ y \ge 0 \text{ and } 0 \le t \le t_W, \\ T = 1, \ \text{for } x = 0, \ y \ge 0 \text{ and } t > t_W, \\ u = v = \frac{\partial T}{\partial x} = 0, \ \text{for } x = 0, \ -0.2 \le y < 0 \\ \dfrac{\partial u}{\partial x} = v = \dfrac{\partial T}{\partial x} = 0, \ \text{for } x = X, \ -0.2 \le y \le Y, \\ \dfrac{\partial^2 u}{\partial y^2} = \dfrac{\partial^2 v}{\partial y^2} = \dfrac{\partial^2 T}{\partial y^2} = 0, \ \text{for } 0 \le x \le X, \ y = Y \\ u = v = \frac{\partial T}{\partial y} = 0, \ \text{for } 0 \le x \le X, \ y = -0.2 \end{array}\right\} \tag{26}$$

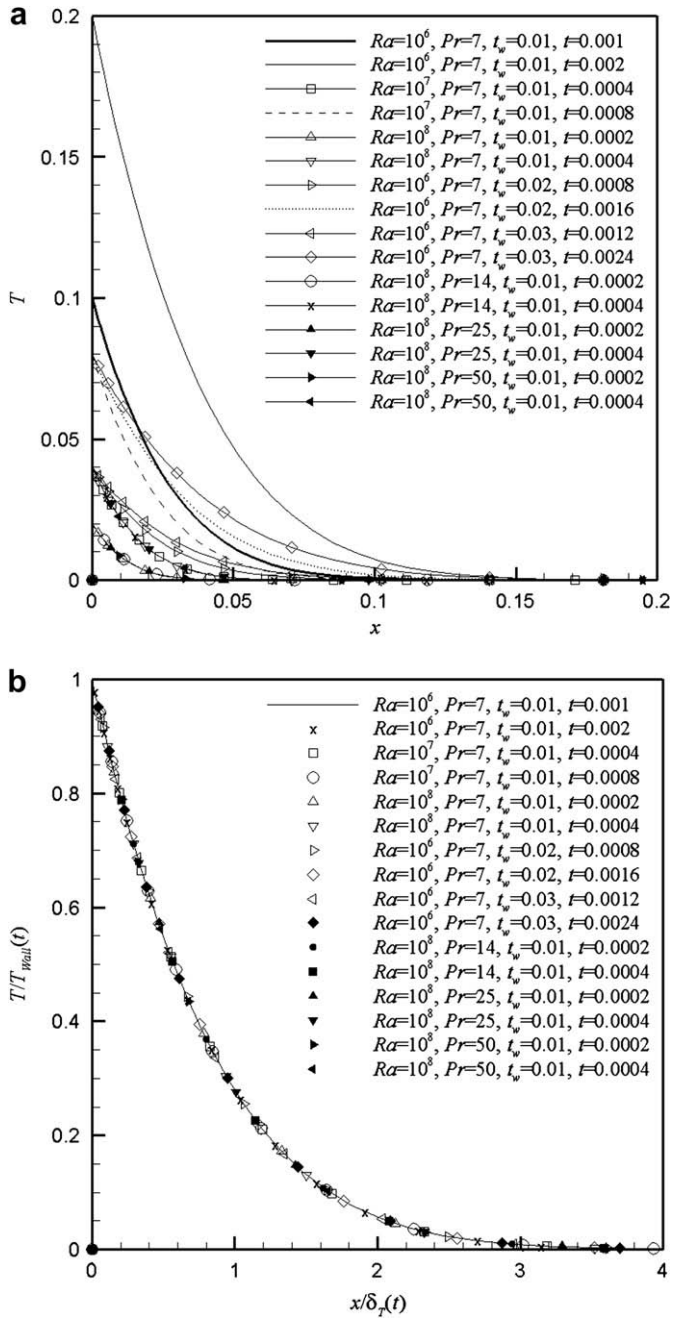

Fig. 2. (a) The unscaled temperature profiles for two times for each of the simulation cases. (b) Scaled temperature profiles plotted against scaled distance for the times in (a). The profiles are for the case $0 < t < t_0$.

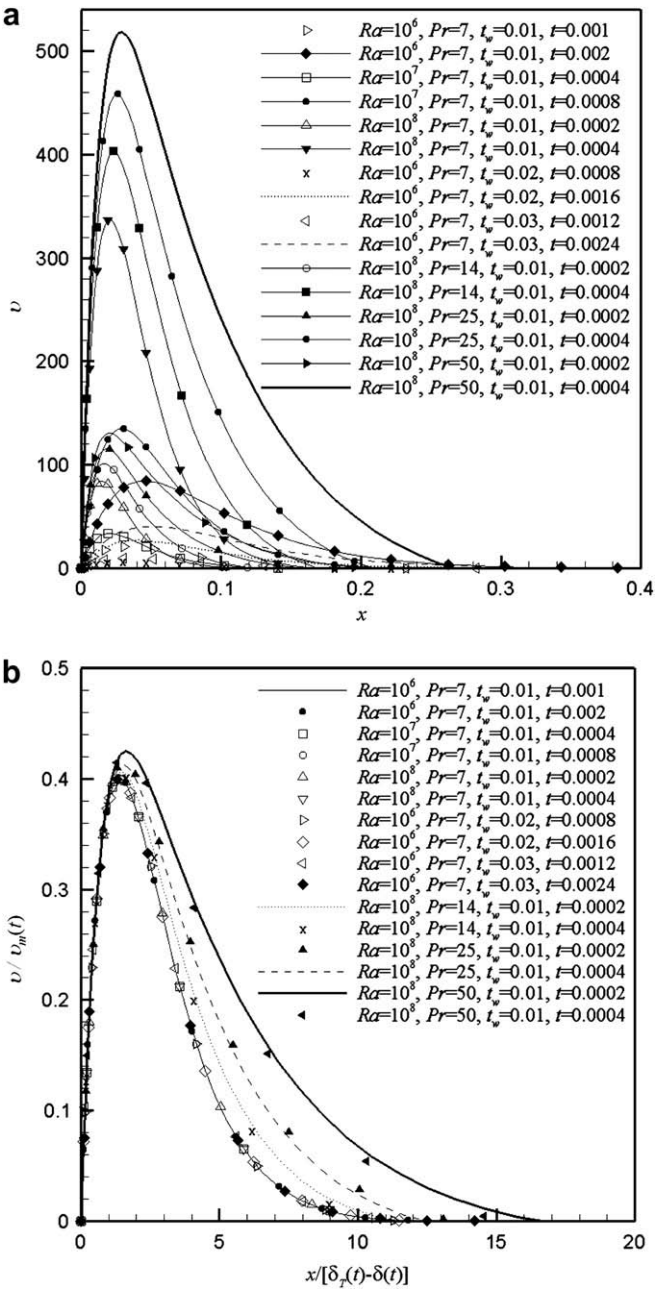

Fig. 3. (a) The unscaled velocity profiles for the same two times as in Fig. 2 for each of the simulation cases. (b) Scaled velocity profiles plotted against the position scaled by the location of the velocity maximum for the times in (a). The profiles are for the case $0 < t < t_0$.

These are effectively open boundary conditions for a semi infinite plate configuration, which is appropriate here [5]. The fluid is initially isothermal, at temperature T_0, and quiescent.

The full equations are discretised on a non-staggered mesh using finite volumes, with standard second order central difference schemes used for the viscous, pressure gradient and divergence terms. The QUICK third order upwind scheme [15], which has been widely used for buoyancy affected flows (eg, [24,28]) is used for the advective terms. The second order Adams–Bashforth scheme and the Crank–Nicolson scheme are used for the time integration of the advective terms and the diffusive terms respectively. To enforce continuity, the pressure correction method is used to construct a Poisson's equation which is solved using a preconditioned GMRES method. Detailed descriptions of these schemes are given in [2,3,8], and the resultant code has been widely used for the simulation of a range of buoyancy dominated flows (see eg, [4,6,18]).

The domain is discretised with a non uniform rectangular grid, with the results presented below obtained with $\Delta x = 1.0 \times 10^{-3}$ at the wall, expanding at a maximum rate of 10% away from the wall, and $\Delta y = 1.0 \times 10^{-3}$ at $y = 0$, also expanding at a maximum rate of 10% away from $y = 0$. This gives a grid of 73×131 nodes in the x and y directions respectively for the $Pr = 7$ case, and 136×302 nodes for the other cases. A time step of $\Delta t = 2.0 \times 10^{-8}$ is used for all cases. Grid and time step dependency tests were undertaken, with results obtained with half the minimum grid sizes and expansion rates given above, and half the time steps. The variation between the results was negligible.

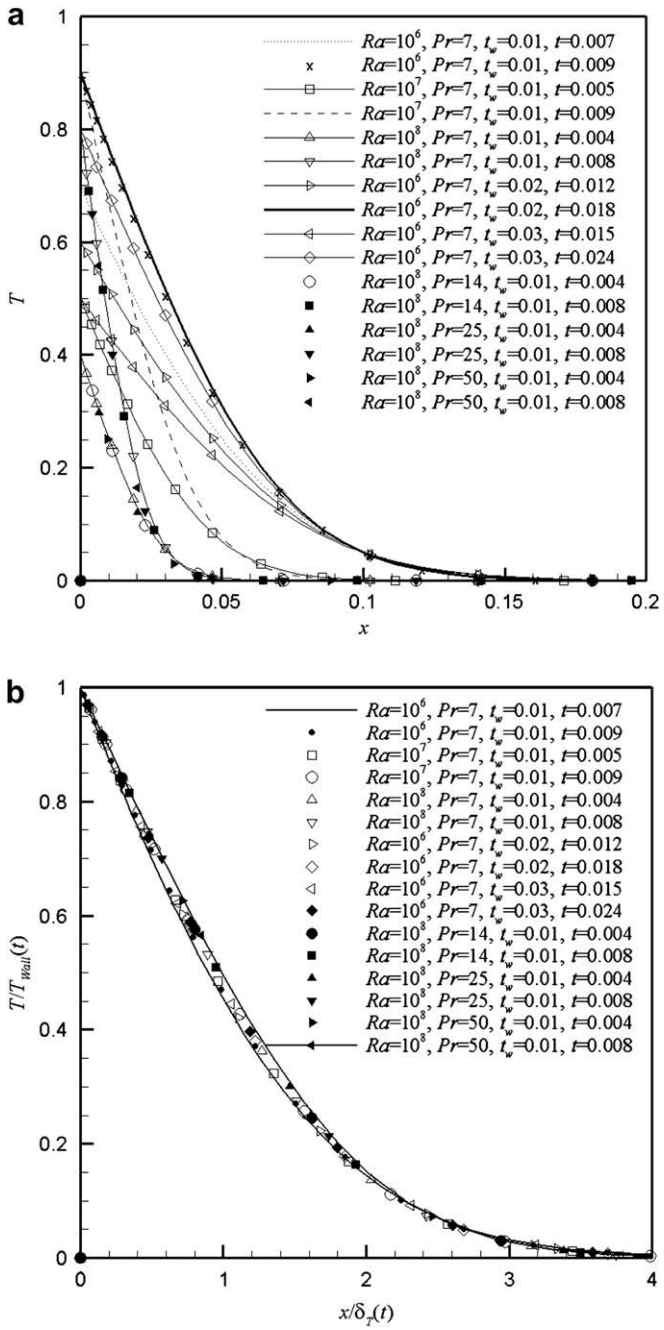

Fig. 4. (a) The unscaled temperature profiles for two times for each of the simulation cases. (b) Scaled temperature profiles plotted against scaled distance for the times in (a). The profiles are for the case $t_0 < t < t_W$.

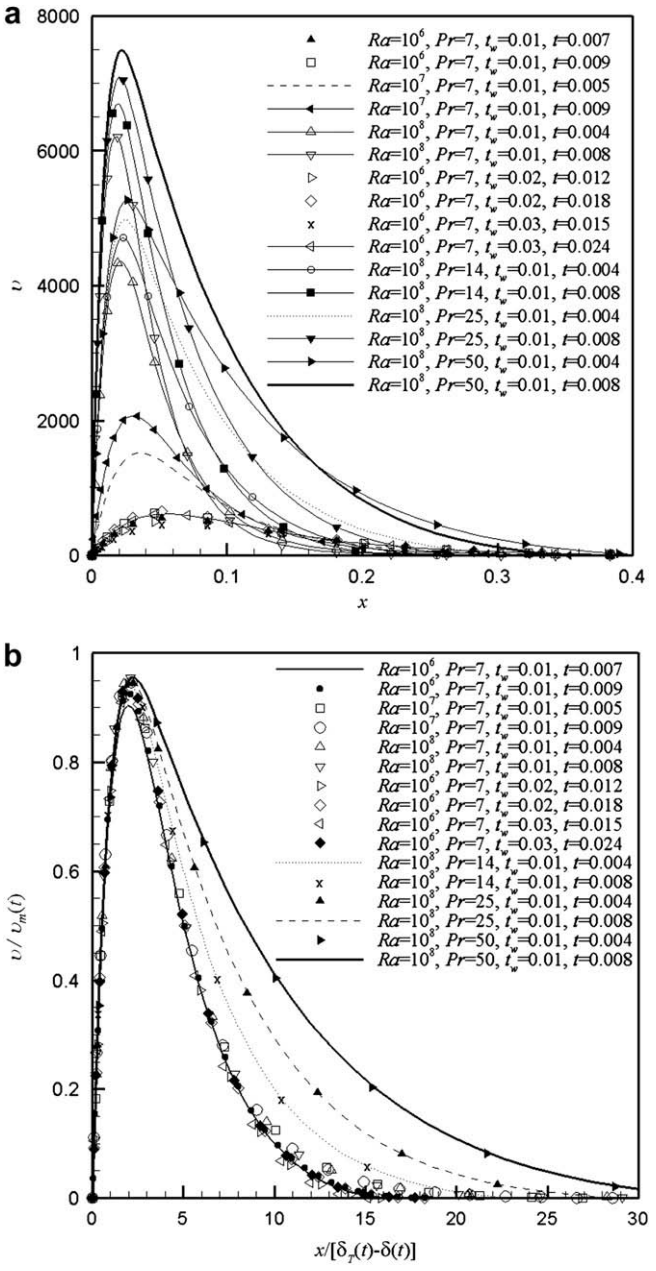

Fig. 5. (a) The unscaled velocity profiles for the same two times as in Fig. 4 for each of the simulation cases. (b) Scaled velocity profiles plotted against the position scaled by the location of the velocity maximum for the times in (a). The profiles are for the case $t_0 < t < t_W$.

In the following, velocity and temperature data are taken at a height $y = 1.0$, which is sufficiently far from the leading edge and the downstream end of the domain to avoid any end effects. Further, the presence or otherwise of travelling waves on the boundary layer associated with the Leading Edge Effect has not been investigated here; that will be the focus of a study which will include an investigation of the stability properties of the boundary layer following this initiation.

5. Results

There are two basic scenarios in the development of the boundary layer with a ramp function boundary condition: first, the case in which the boundary layer reaches a quasi-steady state before the ramp is completed; and second, the case in which the ramp is completed before the boundary layer reaches the quasi-steady state.

As noted above, in the first case, the boundary layer develops following (12) and (17) until the time scale given by (18) is reached. Following this time the boundary layer is in a quasi-steady state, and is described by (22) and (23) until the end of the ramp is reached, at which time the flow becomes steady, described by (24) and (25).

In the second case, the boundary layer follows the development (12) and (17) until the end of the ramp, at which time it follows the description for instantaneous heating until steady state time is

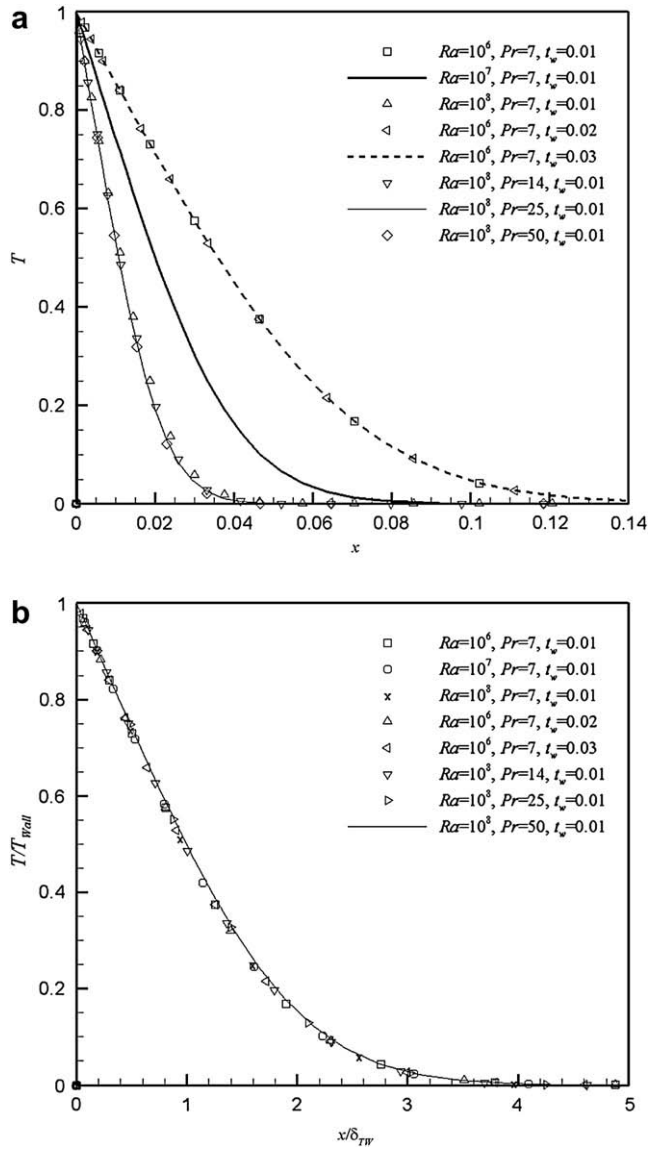

Fig. 6. (a) The unscaled temperature profiles at steady state for all of the simulation cases. (b) The temperature profiles at steady state scaled by the final wall temperature plotted against position scaled by the steady state thermal boundary layer thickness, for all cases.

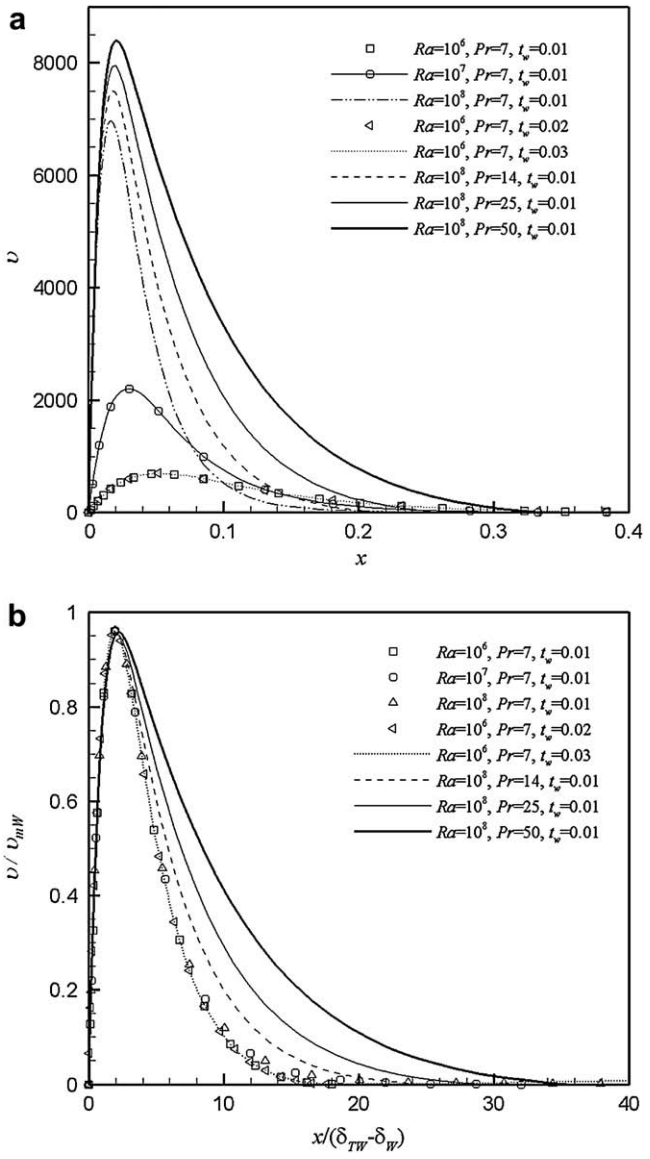

Fig. 7. (a) The unscaled velocity profiles at steady state for all of the simulation cases. (b) The velocity profiles at steady state scaled by the steady state maximum velocity plotted against the position scaled by the location of the velocity maximum, for all cases.

reached, given by (24) and (25). The first part of the development up to time t_W is identical to the first case and the period following t_W up until t_C is described by [19] as part of the development of the instantaneous start up. The steady state in both cases is the same. Since the first stage and the steady state are both verified by an examination of the case $t_0 < t_W$, the case $t_0 > t_W$ is not discussed further here. Using the non dimensionalisation given above, the following scales apply:

$$\left.\begin{aligned} &\delta_T \sim t^{1/2} \\ &\delta_\nu \sim Pr^{1/2}\delta_T \\ &\delta_T - \delta \sim \delta_T\left(1-\tfrac{1}{1+Pr^{1/2}}\right) \\ &\upsilon_m \sim Ra\tfrac{t^2}{t_W}\left(1-\tfrac{1}{1+Pr^{1/2}}\right)^2 \end{aligned}\right\} \text{for } t < t_0 \sim \frac{t_W^{1/3}}{Ra^{1/3}} \frac{1}{\left(1-\frac{1}{1+Pr^{1/2}}\right)^{2/3}} \tag{27}$$

$$\left.\begin{aligned} &\delta_{T0} \sim t_0^{1/2} \\ &\delta_{\nu 0} \sim Pr^{1/2}\delta_{T0} \\ &\delta_{T0} - \delta_0 \sim \delta_{T0}\left(1-\tfrac{1}{1+Pr^{1/2}}\right) \\ &\upsilon_{m0} \sim \tfrac{Ra^{1/3}}{t_W^{1/3}}\left(1-\tfrac{1}{1+Pr^{1/2}}\right)^{2/3} \end{aligned}\right\} \text{for } t \sim t_0 \tag{28}$$

$$\left.\begin{aligned} &\delta_T \sim \frac{1}{Ra^{1/4}\left(1-\frac{1}{1+Pr^{1/2}}\right)^{1/2}}\left(\tfrac{t_W}{t}\right)^{1/4} \\ &\delta_\nu \sim Pr^{1/2}\delta_T \\ &\delta_T - \delta \sim \delta_T\left(1-\tfrac{1}{1+Pr^{1/2}}\right) \\ &\upsilon_m \sim Ra^{1/2}\left(1-\tfrac{1}{1+Pr^{1/2}}\right)\left(\tfrac{t}{t_W}\right)^{1/2} \end{aligned}\right\} \text{for } t_0 < t < t_W \tag{29}$$

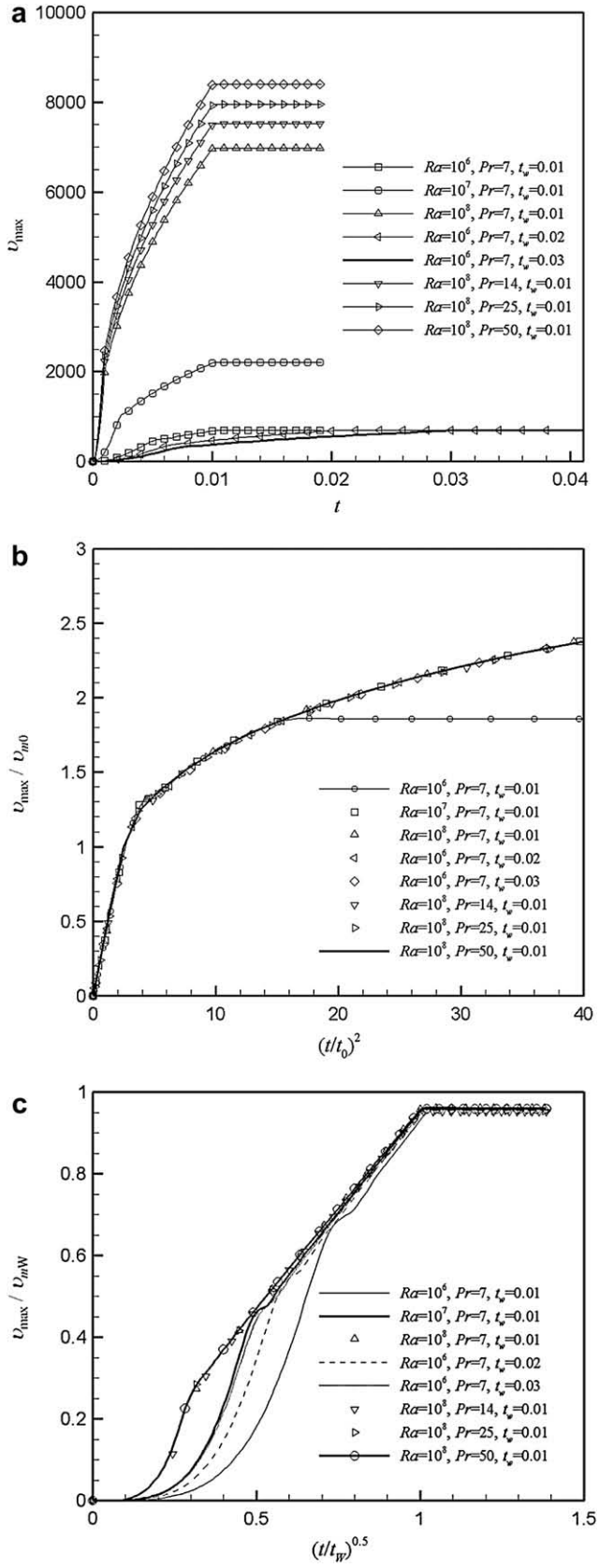

Fig. 8. Time histories of the maximum velocity in the boundary layer for all simulations. (a) Unscaled velocities. (b) Velocities scaled by υ_{m0}, the velocity scale value at the time t_0 at which a quasi-steady state is reached, plotted against $(t/t_0)^2$. (c) Velocities scaled by the steady state value υ_{mW} plotted against $(t/t_W)^{1/2}$.

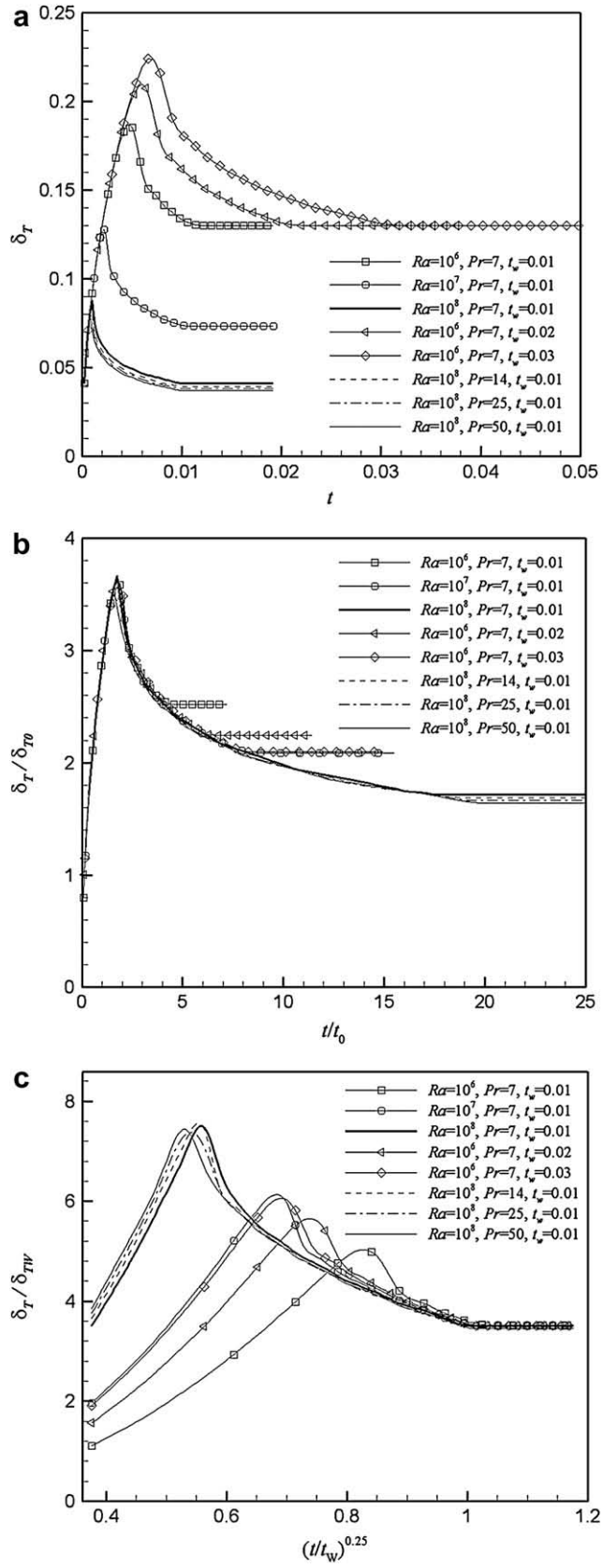

Fig. 9. Time histories of the thermal boundary layer thickness for all simulations. (a) Unscaled thickness plotted against t. (b) The thickness scaled against the value at t_0 plotted against t/t_0. (c) The thickness scaled against the steady state scale plotted against $(t/t_W)^{1/4}$.

$$\left.\begin{array}{l}\delta_{TW} \sim \dfrac{1}{Ra^{1/4}\left(1-\frac{1}{1+Pr^{1/2}}\right)^{1/2}} \\ \delta_{vW} \sim Pr^{1/2}\delta_{TW} \\ \delta_{TW}-\delta_W \sim \delta_{TW}\left(1-\frac{1}{1+Pr^{1/2}}\right) \\ \upsilon_{mW} \sim Ra^{1/2}\left(1-\frac{1}{1+Pr^{1/2}}\right)\end{array}\right\} \text{for } t \geq t_W \quad (30)$$

where all of the variables are non dimensional, and the scales now depend only on *Ra, Pr, t* and t_W.

The non dimensional wall temperature is given by

$$\begin{array}{l} T_{Wall} = 0 \quad t < 0 \\ T_{Wall} = \frac{t}{t_W} \quad 0 \leq t \leq t_W \\ T_{Wall} = 1 \quad t_W < t \end{array} \quad (31)$$

Simulations over the ranges of *Ra, Pr* and t_W reported in Table 1 have been undertaken with the view of spanning the possible regimes and verifying the various scaling relationships given above. These include variations in all of *Ra, Pr* and t_W. The *Ra* and *Pr* values are chosen so that the ratio t_0/t_W lies between 0.05 and 0.27, to ensure that $t_0 < t_W$ and that the ranges $0 < t < t_0$ and $t_0 < t < t_W$ are clearly identifiable, and a range of *Pr* values ($7 < Pr < 50$) and *Ra* values ($10^6 < Ra < 10^8$) are explored.

Consider first the time period $0 < t < t_0$. In this period, two time instants less than t_0 are chosen arbitrarily from each simulation. Fig. 2(a) shows a group of temperature profiles, two from each of the simulated cases. Here the non dimensional temperature is plotted against the non dimensional position. Clearly, the boundary layer thickness in each case increases with time, and the wall temperature also increases with time, as expected.

Fig. 2(b) shows the same data in which the horizontal position has been scaled by the thermal boundary layer thickness δ_T, given by (27), at the appropriate times, and the temperature has been scaled by the wall temperature (31), also at the given times. These profiles are virtually indistinguishable, verifying the thickness scaling.

Fig. 3(a) shows a group of non dimensionalised but unscaled velocity profiles, two from each simulation at the same times as used in Fig. 2. In Fig. 3(b), the vertical velocity is scaled by the transient velocity scale υ_m at the appropriate times, given by (27), and the position is scaled by the position, at the appropriate times, of the maximum velocity ($\delta_T - \delta$), also given by (27), to test scaling for the velocity maximum and its position. Both appear to be well represented by the scaling, within acceptable limits. Consequently, the scales (27) are verified by the simulation results. These same results could have been achieved with any other combinations of times selected, so long as the time is not too close to t_0.

In the time period $t_0 < t < t_W$ the flow is in a quasi steady mode, and is governed by the scales (29). Figs. 4 and 5 present the temperature and velocity profiles from two arbitrary selected times for each case in the same way as Figs. 2 and 3; that is, temperature is scaled by the wall temperature at the appropriate times, the velocity is scaled by the velocity scale at the appropriate times, and the position by the same length scales as in Figs. 2 and 3, again at the appropriate times, all taken from (29). Once again, the strong coincidence of the scaled results verifies the scaling for the boundary layer thickness scales, the position of the velocity maximum and the maximum velocity in this second stage of the flow development.

Table 1
Details of the computations.

Run	t_W	*Pr*	*Ra*	t_0	t_0/t_W
1	0.01	7	10^6	2.7×10^{-3}	0.27
2	0.01	7	10^7	1.2×10^{-3}	0.12
3	0.01	7	10^8	5.7×10^{-4}	0.06
4	0.02	7	10^6	3.4×10^{-3}	0.17
5	0.03	7	10^6	3.8×10^{-3}	0.13
6	0.01	14	10^8	5.4×10^{-4}	0.05
7	0.01	25	10^8	5.2×10^{-4}	0.05
8	0.01	50	10^8	5.1×10^{-4}	0.05

For $t > t_W$, the boundary layer is in a steady state. Figs. 6 and 7 show the profiles of temperature and velocity for an arbitrarily selected time for $t > t_W$. In this case, the temperature is scaled by the steady value of T_{Wall}; the velocity is scaled by υ_{mW} from (30). The length scales used in the scaled plots are the steady state values of δ_T and $\delta_T - \delta$ (δ_{TW} and $\delta_{TW} - \delta_W$) for Figs. 6(b) and 7(b) respectively. Once again, the steady state temperature, velocity and thickness scales are confirmed by the simulation results.

The overall time history is shown in Figs. 8 and 9. In Fig. 8(a), the non dimensionalised maximum velocities υ_{max} from all 8 simulations are shown. The three stages of the flow are clearly shown; the initial development, the quasi-steady stage, and steady state. In the first stage, the velocity varies with t^2 up until t_0, when the velocity is υ_{m0}, given by (28). Fig. 8(b) shows the velocity scaled by υ_{m0}, plotted against $(t/t_0)^2$; clearly the first part of the plot is linear, indicating that the time variation is correct. Further, all of the time series lie together, confirming the scaling for velocity in this stage. The location of the end of the first stage on this plot in each case coincides, confirming that the scaling for t_0 is correct. On this time scaling, only one of the time series shows the transition to the steady state. In the second stage, the velocity varies with $t^{1/2}$; Fig. 8(c) shows the velocity scaled by the steady state value υ_{mW} given by (30), plotted against $(t/t_W)^{1/2}$. Once again the plots show a linear dependence on $(t/t_W)^{1/2}$ as expected during the second part of the development. The location of the start of the second stage at $t \sim t_0$ of course varies in this plot in which time is scaled by t_W. Fig. 8(c) also serves to demonstrate that the steady state velocity is predicted, with all of the time series coinciding past $t/t_W \sim 1$.

Fig. 9 gives the time history of the thermal boundary layer thickness. The computed thickness has been determined by taking the position where the temperature signal is 1% of the wall value. Here the scaling suggests that the boundary layer thickness initially increases as $t^{1/2}$ until the time is t_0, and then decreases as $t^{-1/4}$. Fig. 9(a) shows the non dimensional boundary layer thickness plotted against non dimensional time; the behaviour suggested clearly occurs. When the thickness is scaled by the scale value at t_0, that is δ_{T0}, given by (28), and the time scaled by t_0, as shown in Fig. 9(b), the plots all lie together until the end of the ramp at t_W occurs, when the layer thickness becomes constant. This occurs at different values of t/t_0, and the occurrence of steady state can clearly be observed. Fig. 9(c) shows the dependence of the thickness, scaled by the steady state thickness δ_{TW}, plotted against $(t/t_W)^{1/4}$. This demonstrates, firstly, that the plots for all of the simulations lie together and have a linear dependence on $(t/t_W)^{1/4}$ for the quasi-steady stage (that is for $t_0 < t < t_W$) as predicted by (29), noting that in this scaling the values of t_0/t_W do not coincide for the different cases; and secondly, that all of the steady state values lie together for $t > t_W$, as predicted by (30). Clearly the scales for the boundary layer thickness dependence on time have been confirmed by the simulations.

6. Conclusions

The value of scaling arguments lies in the ability to use the scales derived to estimate the various properties of the flows, and the dependence of the flows on the various parameters. In particular, the success of a scaling analysis of a complex flow means that the various balances in the various stages of the development of the flow have been correctly identified, leading to an understanding of the mechanisms of the flow.

This relies on verification of the scaling, usually by numerical simulation. By varying all of the parameters and examining the simulation data in a scaled way, the coincidence of the scaled results confirms that the scaling developed is correct.

In this paper the case of the start up of the boundary layer on a vertical plate after heating which follows a linear increase in temperature difference up to the final value ΔT over a prescribed time period t_W, that is, a ramp start up, has been examined for a fluid with $Pr \gg 1$. This is in contrast to the case of an instantaneous start up. The characteristic of the ramp start up is that, if the ramp is sufficiently short, then the development follows a particular path until the end of the ramp and then develops as though the start up were instantaneous. In other words, if the ramp is short enough, the flow is indistinguishable from the instantaneous start up case, as might be expected.

On the other hand, if the ramp time is sufficiently long, the flow follows a path of development up until it reaches a quasi-steady state, in which the further development is described by the maintenance of a balance between the conduction of heat through the wall and the convection away by the flow. This is characterized by a boundary layer which slowly accelerates but shrinks in thickness until the end of the ramp. Once the end of the ramp is reached, the flow is steady, and again the flow is identical to that ultimately achieved from an instantaneous start up. So, although the final result is the same, the ramp start up follows a distinctly different path to that state. This different development may have implications for the stability properties of the transient boundary layer, or for the development of the flow in a cavity of which one wall is heated in this way.

The scaling analysis here is only valid for $Pr \gg 1$; for $Pr < 1$ different mechanisms will be involved. Development and analysis of that case is presently underway.

Acknowledgement

The authors gratefully acknowledge the financial support of the Australian Research Council.

References

[1] T. Aberra, S.W. Armfield, M. Behnia, Prandtl number scaling of the natural convection flow over an evenly heated vertical plate ($Pr > 1$), in: Proceedings of CHT-08, ICHMT International Symposium on Advances in Computational Heat Transfer, May 11–16, 2008, Marrakech, Morocco, CHT-08-363.
[2] S.W. Armfield, Finite difference solutions of the Navier–Stokes equations on staggered and non-staggered grids, Comput. Fluid. 20 (1991) 1–17.
[3] S.W. Armfield, Ellipticity, accuracy and convergence of the discrete Navier–Stokes equations, J. Comput. Phys. 114 (1994) 176–184.
[4] S.W. Armfield, W. Debler, Purging of density stabilized basins, Int. J. Heat Mass Transfer 36 (1993) 519–530.
[5] S.W. Armfield, J.C. Patterson, W. Lin, Scaling investigation of the natural convection boundary layer on an evenly heated plate, Int. J. Heat Mass Transfer 50 (2007) 1592–1602.
[6] S.W. Armfield, J.C. Patterson, Direct simulation of wave interactions in unsteady natural convection in a cavity, Int. J. Heat Mass Transfer 34 (1991) 929–940.
[7] S.W. Armfield, J.C. Patterson, Wave properties of natural convection boundary layers, J. Fluid Mech. 239 (1992) 195–211.
[8] S.W. Armfield, R. Street, Fractional step methods for the Navier–Stokes equations on non staggered grids, ANZIAM J. 42 (2000) C134–C156.
[9] S.N. Brown, N. Riley, Flow past a suddenly heated vertical plate, J. Fluid Mech. 59 (1973) 225–237.
[10] B. Gebhart, R.L. Mahajan, Instability and transition in buoyancy induced flows, Adv. Appl. Mech. 22 (1982) 231–315.
[11] R.J. Goldstein, D.G. Briggs, Transient free convection about vertical plates and circular cylinders, Trans. ASME: J. Heat Transfer 86 (1964) 490–500.
[12] D.B. Ingham, Flow past a suddenly cooled vertical plate, J. Inst. Math. Appl. 22 (1978) 189–196.
[13] D.B. Ingham, Flow past a suddenly heated vertical plate, Proc. R. Soc. Lond. A 402 (1985) 109–134.
[14] Y. Joshi, B. Gebhart, Transition of transient vertical natural-convection flows in water, J. Fluid Mech. 179 (1987) 407–438.
[15] B.P. Leonard, A stable and accurate convective modelling procedure based on quadratic upstream interpolation, Comput. Meth. Appl. Mech. Eng. 19 (1979) 59–98.
[16] W. Lin, S.W. Armfield, Direct simulation of natural convection cooling in a vertical circular cylinder, Int. J. Heat Mass Transfer 42 (1999) 4117–4130.
[17] W. Lin, S.W. Armfield, Natural convection cooling of rectangular and cylindrical containers, Int. J. Heat Fluid Flow 22 (2001) 72–81.
[18] W. Lin, S.W. Armfield, Long term behaviour of cooling fluid in a vertical cylinder, Int. J. Heat Mass Transfer 48 (2005) 53–66.
[19] W. Lin, S.W. Armfield, J.C. Patterson, C. Lei, Prandtl number scaling of unsteady natural convection boundary layers of $Pr > 1$ fluids under isothermal heating, Phys. Rev. E, under review.
[20] W. Lin, S.W. Armfield, J.C. Patterson, Cooling of a $Pr < 1$ fluid in a rectangular container, J. Fluid Mech. 574 (2007) 85–108.
[21] S. Ostrach, Laminar flows with body forces, in: F.K. Moore (Ed.), Theory of Laminar Flows, Princeton University Press, 1964, pp. 528–718.
[22] J.C. Patterson, T. Graham, W. Schöpf, S.W. Armfield, Boundary layer development on a semi-infinite, suddenly heated vertical plate, J. Fluid Mech. 453 (2002) 39–55.
[23] J.C. Patterson, J. Imberger, Unsteady natural convection in a cavity, J. Fluid Mech. 100 (1980) 65–86.
[24] M.M. Rahman, A. Miettinen, T. Siikonen, Modified SIMPLE formulation on a collocated grid with an assessment of the simplified QUICK scheme, Numer Heat Trans. B - Fundam. 30 (1996) 291–314.
[25] J.A. Schetz, R. Eichhorn, Unsteady natural convection in the vicinity of a doubly infinite vertical plate, Trans. ASME: J. Heat Transfer 84 (1962) 334–338.
[26] S.G. Schladow, Oscillatory motion in a side heated cavity, J. Fluid Mech. 213 (1990) 589–610.
[27] W. Schöpf, J.C. Patterson, Natural convection in a side heated cavity: visualization of the initial flow features, J. Fluid Mech. 295 (1995) 357–379.
[28] S. Thakur, W. Shyy, Some implementation issues of convective schemes for finite volume formulations, Numer Heat Trans. B - Fundam. 24 (1993) 31–55.